(Received 1 July 2025, Accepted 3 August 2025, Scheduled 15 August 2025)

Continuous High-Order Sliding Mode Optimization Control of PMSM Based on STSMO

Junqin Liu[1,*], Zhentong Wang[1], Feng Deng[1], Kaihui Zhao[2], and Xiangfei Li[2]

[1] National Key Laboratory of Power Grid Disaster Prevention and Mitigation (College of Electrical and Information Engineering Changsha University of Science and Technology), Changsha, Hunan 410114, China
[2] College of Electrical and Information Engineering, Hunan University of Technology, Zhuzhou 412007, China

ABSTRACT: Improving only the speed-loop controller in a PMSM drive system is insufficient to address limitations in the current loops, such as integral saturation and severe oscillations. To achieve high-performance current control across the speed-current loop structure, this paper proposes an improved non-singular fast terminal sliding mode continuous composite control (INFTSMC) method, integrated with a fast super-twisting sliding mode observer (STSMO). Firstly, a state-space model of the PMSM speed-current loops is established. Then, speed and current loop controllers are designed using the STSMO within the INFTSMC framework. The fast super-twisting control law is adopted to reduce the number of observer parameters and to mitigate the severe oscillations caused by high gains in conventional sliding mode observers. Finally, the proposed composite control strategy is compared with conventional PI and SMC + SMO controllers through both simulation and RT-LAB experiments. The results demonstrate that the proposed approach significantly enhances the dynamic response performance of the PMSM drive system.

1. INTRODUCTION

Permanent magnet synchronous motor (PMSM) has become a major focus of research in modern industrial and technological fields due to their high-power density and precise control capabilities [1, 2]. However, in practical applications, PMSM control systems face several challenges, including parameter variations, demagnetization faults, and load disturbances [3], which can significantly impact overall performance and system stability [4]. Therefore, developing high-performance control strategies to address these challenges is of great importance [5]. Proportional-integral (PI) controller is widely used due to its simplicity and ease of implementation, but it exhibits limited effectiveness in coping with parameter variations and external disturbances [6]. Sliding mode control (SMC), as a robust nonlinear control technique, offers significant advantages in such scenarios. Its core principle is to simplify controller design via orderreduction compensation [7–9]. This ensures that the system's trajectory rapidly converges to the sliding surface and remains stable within a finite time. As a result, SMC enables fast dynamic response and high-precision tracking, while improving robustness against internal parameter uncertainties and external disturbances.

SMC offers several advantages, including low dependency on model accuracy, strong robustness against nonlinear disturbances, and ease of implementation [8]. Owing to these benefits, SMC has been widely adopted in motor control applications [10]. In [11], a disturbance observer is introduced to alleviate the chattering effects commonly associated with SMC, thereby enhancing both the smoothness and robustness of the control response. In [12], a continuous fast terminal sliding mode control strategy is applied to PMSM drive systems, achieving faster convergence, improved speed tracking accuracy, and increased robustness. This method significantly enhances the system's dynamic response and stability under complex operating conditions, offering a promising solution for high-performance PMSM control. In [13], a second-order super-twisting sliding mode algorithm is proposed to ensure continuous control signal output, effectively reducing the oscillations typically observed in conventional SMC. Additionally, a sliding mode-based weak magnetic control scheme utilizing a super-twisting sliding mode observer (STSMO) is developed to enable accurate real-time observation of motor states [14]. In [15], a control strategy combining disturbance observer compensation with a terminal sliding mode controller is designed to simultaneously enhance system disturbance rejection and minimize steady-state error — two objectives that are traditionally difficult to achieve concurrently.

Most existing studies have focused on improving the speed-loop controller to address the issue of slow speed convergence [16]. However, the d-q axis current loops in PMSM drive systems are still typically controlled using conventional PI controllers, which fail to meet the requirements for high-performance current regulation. To address this limitation, a composite control (INFTSMC) scheme based on a sliding-mode extended state observer (STESMO). A composite control framework combining INFTSMC and STESMO is designed to enhance the overall control performance of the speed and current loops. Experimental comparisons with PI and SMC + SMO control strategies demonstrate that the proposed method significantly improves the dynamic response and robustness of the PMSM drive system.

* Corresponding author: Junqin Liu (ljq2321925777@163.com).

2. MATHEMATICAL MODEL OF PMSM

The mathematical equation of PMSM under ideal operating conditions can be expressed as [17]:

$$\begin{cases} u_d = R_s i_d + L_d \dfrac{di_d}{dt} - \omega_e L_q i_q \\ u_q = R_s i_q + L_q \dfrac{di_q}{dt} + \omega_e \left(L_d i_d + \psi_f\right) \\ T_e = \dfrac{3}{2} n_p \left[\psi_f + \left(L_d - L_q\right) i_d\right] i_q \\ \dfrac{d\omega_e}{dt} = \dfrac{n_p}{J} \cdot \left(T_e - T_L - B\omega_m\right) \end{cases} \tag{1}$$

where i_d, i_q, u_d, u_q are the d-q axis currents and voltages, respectively. L_d, L_q, ψ_f, R_s are the d-q axis inductances, magnetic flux, and stator resistance, respectively. T_e, T_L are the electromagnetic torque and load torque of the PMSM.

In actual engineering applications [18], disturbances affect the dynamic performance and stability of PMSM. Considering the composite perturbation of parameters and external time-varying disturbance conditions, Eq. (1) of PMSM can be rewritten as:

$$\begin{cases} u_d = R_s i_d + \dfrac{d\psi_d}{dt} - \omega_e \psi_q + \Delta u_d \\ u_q = R_s i_q + \dfrac{d\psi_q}{dt} + \omega_e \psi_d + \Delta u_q \\ T_e = \dfrac{3}{2} n_p \left[\psi_f + (L_d - L_q) i_d\right] i_q + \Delta T_e \\ \dfrac{d\omega_e}{dt} = \dfrac{3n_p^2}{2J} \psi_e i_q + \begin{bmatrix} -\frac{B}{J}\omega_e + \Delta P_n + \Delta D \\ +\frac{n_p}{J} \cdot (\Delta T_e - T_L + \Delta T_L) \end{bmatrix} \end{cases} \tag{2}$$

where ΔD is the "unmodeled dynamics" in the system. Δu_d, Δu_q, ΔT_e, and ΔP_n are disturbance quantities.

3. DESIGN OF INFTSMC BASED ON STSMO

3.1. Speed-Current Loops Model of PMSM

The first-order nonlinear model [19] can be expressed as

$$\begin{cases} y = x \\ \dfrac{dx}{dt} = \lambda_1 u + \lambda_2 x + F \end{cases} \tag{3}$$

where $x \in \Re$, $\lambda_1 \in \Re$; y and u are the system output and input; λ_2 is the gain to be designed; F is the unknown part.

Combining Eq. (2) and Eq. (3), the speed-current-loops model for the PMSM is designed as:

$$\begin{cases} \dfrac{d\omega_e}{dt} = \lambda_{1\omega} i_q + \lambda_{2\omega} \omega_e + F_\omega \\ \dfrac{di_d}{dt} = \lambda_{1d} u_d + \lambda_{2d} i_d + F_d \\ \dfrac{di_q}{dt} = \lambda_{1q} u_q + \lambda_{2q} i_q + F_q \end{cases} \tag{4}$$

Equation (4) can be designed as

$$\dot{\mathbf{x}} = \boldsymbol{\lambda}_1 \mathbf{u} + \boldsymbol{\lambda}_2 \mathbf{x} + \mathbf{F} \tag{5}$$

where $\mathbf{u} = \begin{bmatrix} i_q & u_d & u_q \end{bmatrix}^{\mathrm{T}}$, $\mathbf{x} = \begin{bmatrix} \omega_e & i_d & i_q \end{bmatrix}^{\mathrm{T}}$, $\mathbf{F} = \begin{bmatrix} F_\omega & F_d & F_q \end{bmatrix}^{\mathrm{T}}$, $\boldsymbol{\lambda}_1 = diag(\lambda_{1\omega}, \lambda_{1d}, \lambda_{1q})$, $\boldsymbol{\lambda}_2 = diag(\lambda_{2\omega}, \lambda_{2d}, \lambda_{2q})$.

3.2. Design of INFTSMC

According to Eq. (4), the control laws for PMSM speed-current loops are designed as follows:

$$\begin{cases} i_q^* = \dfrac{\dot{\omega}_e - \lambda_{2\omega}\omega_e + u_{1\omega} + F_\omega}{\lambda_{1\omega}} \\ u_d^* = \dfrac{\dot{i}_d - \lambda_{2d} i_d + u_{1d} + F_d}{\lambda_{1d}} \\ u_q^* = \dfrac{\dot{i}_q - \lambda_{2q} i_q + u_{1q} + F_q}{\lambda_{1q}} \end{cases} \tag{6}$$

Equation (6) can be designed as

$$\mathbf{u}^* = \frac{\dot{\mathbf{x}}^* - \boldsymbol{\lambda}_2 \mathbf{x} + \mathbf{u_1} + \mathbf{F}}{\boldsymbol{\lambda}_1} \tag{7}$$

where $\mathbf{u}^* = \begin{bmatrix} i_q^* & u_d^* & u_q^* \end{bmatrix}^{\mathrm{T}}$, $\mathbf{x}^* = \begin{bmatrix} \omega_e^* & i_d^* & i_q^* \end{bmatrix}^{\mathrm{T}}$, $\mathbf{u_1} = \begin{bmatrix} u_{1\omega} & u_{1d} & u_{1q} \end{bmatrix}^{\mathrm{T}}$. $\mathbf{u}^*$ and $\mathbf{x}^*$ are given values for the system, and $\mathbf{u_1}$ represents the output of the controllers.

Substituting Eq. (7) into Eq. (5), $\dot{\mathbf{e}} = -\mathbf{u}_1$. The state errors are $e_\omega = \omega_e^* - \omega_e$, $e_d = i_d^* - i_d$, $e_q = i_q^* - i_q$:

$$\mathbf{e} = \mathbf{x}^* - \mathbf{x} \tag{8}$$

where $\mathbf{e} = \begin{bmatrix} e_\omega & e_d & e_q \end{bmatrix}^{\mathrm{T}}$, $\mathbf{x}^* = \begin{bmatrix} \omega_e^* & i_d^* & i_q^* \end{bmatrix}^{\mathrm{T}}$, $\mathbf{x} = \begin{bmatrix} \omega_e & i_d & i_q \end{bmatrix}^{\mathrm{T}}$.

Defining $\dot{\mathbf{e}}_1 = \mathbf{e_2}$, $\dot{\mathbf{e}}_2 = \dot{\mathbf{e}}$, designing $\mathbf{s}$ as [21]:

$$\mathbf{s} = \mathbf{e_1} + \mathbf{a_1} \mathbf{e}_1^{l_1} + \mathbf{a_2} \mathbf{e}_2^{l_2} + \mathbf{e_2} \tag{9}$$

where $\mathbf{a_1} = diag(a_{1\omega}, a_{1d}, a_{1q})$, $a_{1\omega} > 0$, $a_{1d} > 0$, $a_{1q} > 0$. $\mathbf{a_2} = diag(a_{2\omega}, a_{2d}, a_{2q})$, $a_{2\omega} > 0$, $a_{2d} > 0$, $a_{2q} > 0$. $l_1 = p/q$, $l_2 = g/h$, $g > 0$, $h > 0$, $p > 0$, $q > 0$, $1 < l_1 < 2$, $l_2 > l_1$.

Take the derivative of Eq. (9):

$$\begin{aligned} \dot{s} &= \dot{e}_1 + \mathbf{a}_1 l_1 \mathbf{e}_1^{l_1 - 1} e_2 + \mathbf{a}_2 l_2 \mathbf{e}_2^{l_2 - 1} \dot{e}_2 + \dot{e}_2 \\ &= \dot{e}_2 + \mathbf{a}_1 l_1 \mathbf{e}_1^{l_1 - 1} e_2 + \left(\mathbf{a}_2 l_2 \mathbf{e}_2^{l_2 - 1} + 1\right) \dot{e}_2 \end{aligned} \tag{10}$$

The index convergence law [21] is

$$\dot{\mathbf{s}} = -\boldsymbol{\eta}_1 \mathrm{sgn}(\mathbf{s}) - \boldsymbol{\eta}_2 \mathbf{s} \tag{11}$$

where $\boldsymbol{\eta}_1 = diag(\eta_{1\omega}, \eta_{1d}, \eta_{1q})$, $\eta_{1\omega} > 0$, $\eta_{1d} > 0$, $\eta_{1q} > 0$. $\boldsymbol{\eta_2} = diag(\boldsymbol{\eta}_{2\omega}, \boldsymbol{\eta}_{2d}, \boldsymbol{\eta}_{2q})$, $\eta_{2\omega} > 0$, $\eta_{2d} > 0$, $\eta_{2q} > 0$.

From Eq. (10), the equivalent control law for sliding mode surface $\mathbf{u_{1e}}$ is

$$\mathbf{u_{1e}} = \left(1 + \mathbf{a}_2 l_2 \mathbf{e}_2^{l_2 - 1}\right)^{-1} \cdot \left(\mathbf{e}_2 + \mathbf{a}_1 l_1 \mathbf{e}_2 \mathbf{e}_1^{l_1 - 1}\right) \tag{12}$$

From Eq. (11), the equivalent control law for index convergence $\mathbf{u_{1q}}$ is

$$\mathbf{u_{1q}} = \boldsymbol{\eta}_1 \mathrm{sgn}(\mathbf{s}) + \boldsymbol{\eta}_2 \mathbf{s} \tag{13}$$

From Eq. (12) and Eq. (13), the equivalent control law for INFTSMC $\mathbf{u_1}$ is

$$\mathbf{u_1} = \mathbf{u}_{1e} + \mathbf{u}_{1q} \tag{14}$$

From Eq. (14) and Eq. (7), the overall control laws $\mathbf{u}^*$ for the INFTSMC speed-current loop controllers can be obtained as:

$$\begin{aligned} \mathbf{u}^* &= \frac{\dot{\mathbf{x}}^* - \boldsymbol{\lambda}_2 \mathbf{x} + \mathbf{u}_1 - \mathbf{F}}{\boldsymbol{\lambda}_1} \\ &= \frac{1}{\boldsymbol{\lambda}_1} \begin{bmatrix} \dot{\mathbf{x}}^* - \boldsymbol{\lambda}_2 \mathbf{x} - \mathbf{F} + \left(1 + \mathbf{a}_2 l_2 \mathbf{e}_2^{l_2 - 1}\right)^{-1} \\ \cdot \left(\mathbf{e}_2 + \mathbf{a}_1 l_1 \mathbf{e}_2 \mathbf{e}_1^{l_1 - 1}\right) + \boldsymbol{\eta}_1 \mathrm{sgn}(\mathbf{s}) + \boldsymbol{\eta}_2 \mathbf{s} \end{bmatrix} \end{aligned} \tag{15}$$

Proof of system stability: Selecting Lyapunov function V as

$$V = \frac{1}{2} s^2 \tag{16}$$

Take the derivative of V:

$$\begin{aligned} \dot{V} &= s \left[e_2 + a_1 l_1 e_1^{l_1 - 1} e_2 + \left(a_2 l_2 e_2^{l_2 - 1} + 1\right) \dot{e}_2 \right] \\ &= s \left[\left(a_2 l_2 e_2^{l_2 - 1} + 1\right) \left(\|\tilde{F}\| - \eta_1 \mathrm{sgn(s)} - \eta_2 \mathrm{s} \right) \right] \\ &\leq \left(a_2 l_2 e_2^{l_2 - 1} + 1\right) \left(\left(\|\tilde{F}\| - \eta_1 \right) \|s\| - \eta_2 \|s\|^2 \right) \end{aligned} \tag{17}$$

while $\boldsymbol{\eta}_1 \geq \left\| \tilde{F} \right\| + \rho \ (\rho > 0)$, $\dot{V} \leq 0$. The convergence time of the INFTSMC is $T_s \leq \ln \left(1 + \exp^{\varepsilon \tau t} \mathbf{V}_{(0)}^{\tau}\right) / \boldsymbol{\varepsilon \tau}$.

3.3. Design of STSMO for INFTSMC

Defining $\mathbf{x} = \hat{\mathbf{x}} - \mathbf{x}_1$, $\hat{\mathbf{x}} = \begin{bmatrix} \hat{\omega}_e & \hat{i}_d & \hat{i}_q \end{bmatrix}^{\mathrm{T}}$, $\mathbf{x}_1 = \begin{bmatrix} \omega_e & i_d & i_q \end{bmatrix}^{\mathrm{T}}$.

Redefine the new equation as

$$\frac{d\hat{\mathbf{x}}}{dt} = \boldsymbol{\lambda_1} \mathbf{u} + \boldsymbol{\lambda_2} \hat{\mathbf{x}} + \mathbf{F} + \mathbf{u}_{stsmo} \tag{18}$$

where $\mathbf{u_{stsmo}} = \begin{bmatrix} u_{stsmo\omega} & u_{stsmod} & u_{stsmoq} \end{bmatrix}^{\mathrm{T}}$, $\hat{\mathbf{F}} = [\hat{F}_\omega \quad \hat{F}_d \quad \hat{F}_q]^T$.

From Eq. (18), Eq. (19) can be expressed as:

$$\frac{d\mathbf{x}}{dt} = \boldsymbol{\lambda_2} \mathbf{x} + \tilde{\mathbf{F}} + \mathbf{u}_{stsmo} \tag{19}$$

where $\tilde{\mathbf{F}} = [\tilde{F}_\omega \quad \tilde{F}_d \quad \tilde{F}_q]^T$, $\tilde{\mathbf{F}} = \hat{\mathbf{F}} - \mathbf{F}$.

Design $\mathbf{s} = \mathbf{s}_1 = \mathbf{x} = \hat{\mathbf{x}} - \mathbf{x}_1$, and design fast super-twisting control law [22] as

$$\dot{\mathbf{s}}_1 = -\mathbf{k}_1 \left|\mathbf{s}_1\right|^{\frac{1}{2}} \mathrm{sgn}\left(\mathbf{s}_1\right) + \mathbf{k}_2 \mathbf{s}_1 - \int \mathbf{k}_3 \mathrm{sgn}\left(\mathbf{s}_1\right) + \mathbf{F} \tag{20}$$

where $\mathbf{k}_1 = diag(k_{1\omega}, k_{1d}, k_{1q})$, $k_{1\omega} > 0$, $k_{1d} > 0$, $k_{1q} > 0$, $\mathbf{k_3} = diag(k_{3\omega}, k_{3d}, k_{3q})$, $k_{3\omega} > 0$, $k_{3d} > 0$. $k_{3q} > 0$, $\mathbf{k}_2 = \boldsymbol{\lambda}_2$.

From Eqs. (18)–(20), the control law for STSMO $\mathbf{u_{stsmo}}$ can be expressed as:

$$\mathbf{u_{stsmo}} = -\mathbf{k}_1 \left|\mathbf{s}_1\right|^{\frac{1}{2}} \mathrm{sgn}\left(\mathbf{s}_1\right) - \int_0^t \mathbf{k}_3 \mathrm{sgn}\left(\mathbf{s}_1\right) dt \tag{21}$$

Proof of system stability: Selecting Lyapunov function $V_1(x)$ as

$$\begin{aligned} V_1(x) &= 2k_3 |s| + \frac{1}{2} g^2 + \frac{1}{2} \dot{s}^2 \\ &= \frac{1}{2} \begin{bmatrix} (4k_3 + k_1^2) |s|^{\frac{1}{2}} \mathrm{sgn}(s) - k_1 k_2 s - k_1 g \\ -k_1 k_2 |s|^{\frac{1}{2}} \mathrm{sgn}(s) + k_2^2 s + k_2 g \\ -k_1 |s|^{\frac{1}{2}} \mathrm{sgn}(s) + k_2 s + 2g \end{bmatrix}^{\mathrm{T}} \\ &\quad \begin{bmatrix} |s|^{\frac{1}{2}} \mathrm{sgn}(s) \\ s \\ g \end{bmatrix} \end{aligned} \tag{22}$$

Equation (22) can be simplified to

$$V_1 = \boldsymbol{\zeta}^{\mathrm{T}} \mathbf{Q} \boldsymbol{\zeta} \tag{23}$$

where $\mathbf{Q} = \frac{1}{2} \begin{bmatrix} (4k_3 + k_1^2) & -k_1 k_2 & -k_1 \\ -k_1 k_2 & k_2^2 & k_2 \\ -k_1 & k_2 & 2 \end{bmatrix}$, $\boldsymbol{\zeta}^{\mathrm{T}} = \begin{bmatrix} |s|^{\frac{1}{2}} \mathrm{sgn}(s) & s & g \end{bmatrix}$.

In Eq. (21), the determinants of the first-order master form $\mathbf{Q}_1$, second-order master form $\mathbf{Q}_2$, and third-order master form $\mathbf{Q}_3$ are

$$\begin{cases} |\mathbf{Q}_1| = \left|4k_3 + k_1^2\right| > 0 \\ |\mathbf{Q}_2| = \begin{vmatrix} 4k_3 + k_1^2 & -k_1 k_2 \\ -k_1 k_2 & k_2^2 \end{vmatrix} > 0 \\ |\mathbf{Q}_3| = \begin{vmatrix} 4k_3 + k_1^2 & -k_1 k_2 & -k_1 \\ -k_1 k_2 & k_2^2 & k_2 \\ -k_1 & k_2 & 2 \end{vmatrix}^2 > 0 \end{cases} \tag{24}$$

From Eq. (24), $\mathbf{Q}$ is a positive definite matrix, and V_1 is a positive definite and continuous function [23]. Applying the chain rule $d|x|/dt = \dot{x}\mathrm{sgn}(x)$ to find $\dot{V}_1$. Take the derivative of $\boldsymbol{\zeta}$:

$$\begin{aligned} \dot{\boldsymbol{\zeta}} &= \begin{bmatrix} |s|^{1/2} \mathrm{sgn}(s) & s & g \end{bmatrix}^{\mathrm{T}} \\ &= \frac{1}{|s|^{1/2}} \cdot \frac{1}{2} \begin{bmatrix} -k_1 & k_2 & 1 \\ 0 & 0 & 0 \\ -2k_3 & 0 & 0 \end{bmatrix} \begin{bmatrix} |s|^{\frac{1}{2}} \mathrm{sgn}(s) \\ s \\ g \end{bmatrix} \end{aligned}$$

$$+\begin{bmatrix} 0 & 0 & 0 \\ -k_1 & k_2 & 1 \\ 0 & 0 & 0 \end{bmatrix}\boldsymbol{\zeta}+\begin{bmatrix} 0 \\ 0 \\ \dot{F} \end{bmatrix}$$

$$= \frac{1}{|s|^{1/2}}\mathbf{W}\boldsymbol{\zeta}+L\zeta+\boldsymbol{\upsilon} \tag{25}$$

where $\mathbf{W}=\frac{1}{2}\begin{bmatrix} -k_1 & k_2 & 1 \\ 0 & 0 & 0 \\ -2k_3 & 0 & 0 \end{bmatrix}$, $\mathbf{L}=\begin{bmatrix} 0 & 0 & 0 \\ -k_1 & k_2 & 1 \\ 0 & 0 & 0 \end{bmatrix}$, $\boldsymbol{\upsilon}=\begin{bmatrix} 0 & 0 & \dot{F} \end{bmatrix}^{\mathrm{T}}$.

Take the derivative of $\dot{V}_1$:

$$\begin{aligned}\dot{V}_1 &= \dot{\boldsymbol{\zeta}}^{\mathrm{T}}\mathbf{Q}\boldsymbol{\zeta}+\boldsymbol{\zeta}^{\mathrm{T}}\mathbf{Q}\dot{\boldsymbol{\zeta}} \\ &= -\frac{1}{|s|^{1/2}}\boldsymbol{\zeta}^{\mathrm{T}}\mathbf{P}_1\boldsymbol{\zeta}-\boldsymbol{\zeta}^{\mathrm{T}}\mathbf{P}_2\boldsymbol{\zeta}+\dot{F}\boldsymbol{\rho}^{\mathrm{T}}\boldsymbol{\zeta} \\ &\leq -\frac{1}{|s|^{1/2}}\boldsymbol{\zeta}^{\mathrm{T}}\mathbf{P}_1\boldsymbol{\zeta}-\boldsymbol{\zeta}^{\mathrm{T}}\mathbf{P}_2\boldsymbol{\zeta}+\delta\boldsymbol{\rho}^{\mathrm{T}}\boldsymbol{\zeta}\end{aligned} \tag{26}$$

where $\rho=[-k_1 \quad k_2 \quad 2]$, $\dot{F}\leq\delta$,

$$P_1=\frac{1}{2}\begin{bmatrix} 2k_1k_3+k_1^3 & (k_1^2+k_3)k_2 & k_1^2 \\ (k_1^2+k_3)k_2 & -k_1k_2^2 & -k_1k_2 \\ k_1^2 & -k_1k_2 & -k_1 \end{bmatrix},$$

$$P_2=k_2\begin{bmatrix} k_1^2 & -k_1k_2 & -k_1 \\ -k_1k_2 & k_2^2 & k_2 \\ -k_1 & k_2 & 1 \end{bmatrix}.$$

The boundary of $\dot{F}$ is

$$\begin{aligned}\dot{\mathbf{F}}\boldsymbol{\rho}^{\mathrm{T}}\boldsymbol{\zeta} &= \dot{F}\begin{bmatrix} -k_1 & k_2 & 2 \end{bmatrix}\begin{bmatrix} |s|^{1/2}\operatorname{sgn}(s) \\ s \\ g \end{bmatrix} \\ &= \frac{\dot{F}}{|s|^{1/2}}\begin{bmatrix} -k_1|s|^{1/2}\cdot|s|^{1/2}\operatorname{sgn}(s) \\ +k_2s|s|^{1/2}+g\cdot|s|^{1/2}+g\cdot|s|^{1/2} \end{bmatrix} \\ &= \frac{1}{|s|^{1/2}}\boldsymbol{\zeta}^{\mathrm{T}}\mathbf{M_1}\boldsymbol{\zeta}+\boldsymbol{\zeta}^{\mathrm{T}}\mathbf{M_2}\boldsymbol{\zeta}\end{aligned} \tag{27}$$

where $\mathbf{M_1}=\begin{bmatrix} -k_1\dot{F}\operatorname{sgn}(s) & 0 & \dot{F}\operatorname{sgn}(s) \\ 0 & k_2\dot{F} & 0 \\ \dot{F}\operatorname{sgn}(s) & 0 & 0 \end{bmatrix}$,

$\mathbf{M_2}=\begin{bmatrix} -k_2\dot{F}\operatorname{sgn}(s) & 0 & 0 \\ 0 & 0 & 0 \\ 0 & 0 & 0 \end{bmatrix}$.

Substitute Eq. (27) into Eq. (26):

$$\begin{aligned}\dot{V}_1 &= -\frac{1}{|s|^{1/2}}\boldsymbol{\zeta}^{\mathrm{T}}\mathbf{P}_1\boldsymbol{\zeta}-\boldsymbol{\zeta}^{\mathrm{T}}\mathbf{P}_2\boldsymbol{\zeta}+\frac{1}{|s|^{1/2}}\boldsymbol{\zeta}^{\mathrm{T}}\mathbf{M_1}\boldsymbol{\zeta}+\boldsymbol{\zeta}^{\mathrm{T}}\mathbf{M_2}\boldsymbol{\zeta} \\ &= -\frac{1}{|s|^{1/2}}\boldsymbol{\zeta}^{\mathrm{T}}\left(\mathbf{P}_1-\mathbf{M_1}\right)\boldsymbol{\zeta}-\boldsymbol{\zeta}^{\mathrm{T}}\left(\mathbf{P}_2-\mathbf{M_2}\right)\boldsymbol{\zeta}\end{aligned} \tag{28}$$

From Eq. (28), while $\mathbf{P}_1-\mathbf{M}>0$ and $\mathbf{P}_2-\mathbf{M_2}>0$, $\dot{V}_1<0$. The necessary and sufficient condition for $\mathbf{P}_1-\mathbf{M}>0$ is

$$\begin{cases} k_1^2+2k_3+2\dot{F}\operatorname{sgn}(s)>0 \\ k_2^2(k_3^2-2k_1^2\dot{F}\operatorname{sgn}(s))>0 \\ k_2^2(9k_1^2+8k_3+28\dot{F}\operatorname{sgn}(s)+20\dot{F}^2/k_1^2)<0 \end{cases} \tag{29}$$

The necessary and sufficient condition for $\mathbf{P}_2-\mathbf{M_2}>0$ is

$$\begin{cases} 2k_1^2+\dot{F}\operatorname{sgn}(s)>0 \\ k_1^2+\dot{F}\operatorname{sgn}(s)-k_1^2k_2>0 \end{cases} \tag{30}$$

From Eq (29) and Eq. (30):

$$\lambda_{\min}(\mathbf{Q})\|\boldsymbol{\zeta}\|^2<V_1<\lambda_{\max}(\mathbf{Q})\|\boldsymbol{\zeta}\|^2 \tag{31}$$

From the quadratic standard inequality, we can see that

$$|s|^{1/2}\leq\|\boldsymbol{\zeta}\|\leq V_1^{1/2}/\lambda_{\min}^{1/2}(\mathbf{Q}) \tag{32}$$

where $\|\boldsymbol{\zeta}\|=\sqrt{|s|+|s|^2+|g|^2}$.

In summary, it can be concluded that

$$\begin{aligned}\dot{V}_1 &= -\frac{1}{|s|^{1/2}}\boldsymbol{\zeta}^{\mathrm{T}}\left(\mathbf{P}_1-\mathbf{M_1}\right)\boldsymbol{\zeta}-\boldsymbol{\zeta}^{\mathrm{T}}\left(\mathbf{P}_2-\mathbf{M_2}\right)\boldsymbol{\zeta} \\ &\leq -\mu_1V_1^{1/2}-\mu_2V_1^{1/2} \\ &\leq -\mu_1V_1^{1/2} \\ &\leq 0\end{aligned} \tag{33}$$

where $\mu_1=\left[\lambda_{\min}^{1/2}(\mathbf{Q})\,\delta\left(\mathbf{P}_1-\mathbf{M_1}\right)\right]/\lambda_{\max}^{1/2}(\mathbf{Q})$, $\mu_2=\lambda_{\min}^{1/2}(\mathbf{P}_2-\mathbf{M_2})/\lambda_{\max}(\mathbf{Q})$, $\lambda_{\min}(\mathbf{Q})$ and $\lambda_{\max}(\mathbf{Q})$ are the minimum and maximum eigenvalues of $\mathbf{Q}$, respectively.

From Eq. (33), the designed STSMO satisfies the Lyapunov stability theorem [24]. From Eq. (19) and Eq. (21), the expression for $\hat{F}$ is shown in Eq. (34):

$$\hat{\mathbf{F}}=\mathbf{k}_1|\mathbf{s}_1|^{\frac{1}{2}}\operatorname{sgn}(\mathbf{s}_1)+\int_0^t\mathbf{k}_3\operatorname{sgn}(\mathbf{s}_1)\,dt \tag{34}$$

Therefore, the total control law $\mathbf{u}^*$ of INFTSMC + STSMO is expressed as:

$$\begin{aligned}\mathbf{u}^* &= \frac{\dot{\mathbf{x}}^*-\boldsymbol{\lambda}_2\mathbf{x}+\mathbf{u}_1-\hat{\mathbf{F}}}{\boldsymbol{\lambda}_1} \\ &= \frac{1}{\boldsymbol{\lambda}_1}\begin{bmatrix} \dot{\mathbf{x}}^*-\boldsymbol{\lambda}_2\mathbf{x}-\hat{\mathbf{F}}+\left(1+\mathbf{a}_2l_2\mathbf{e}_2^{l_2-1}\right)^{-1} \\ \cdot\left(\mathbf{e}_2+\mathbf{a}_1l_1\mathbf{e}_2\mathbf{e}_1^{l_1-1}\right)+\boldsymbol{\eta}_1\operatorname{sgn}(\mathbf{s})+\boldsymbol{\eta}_2\mathbf{s} \end{bmatrix}\end{aligned} \tag{35}$$

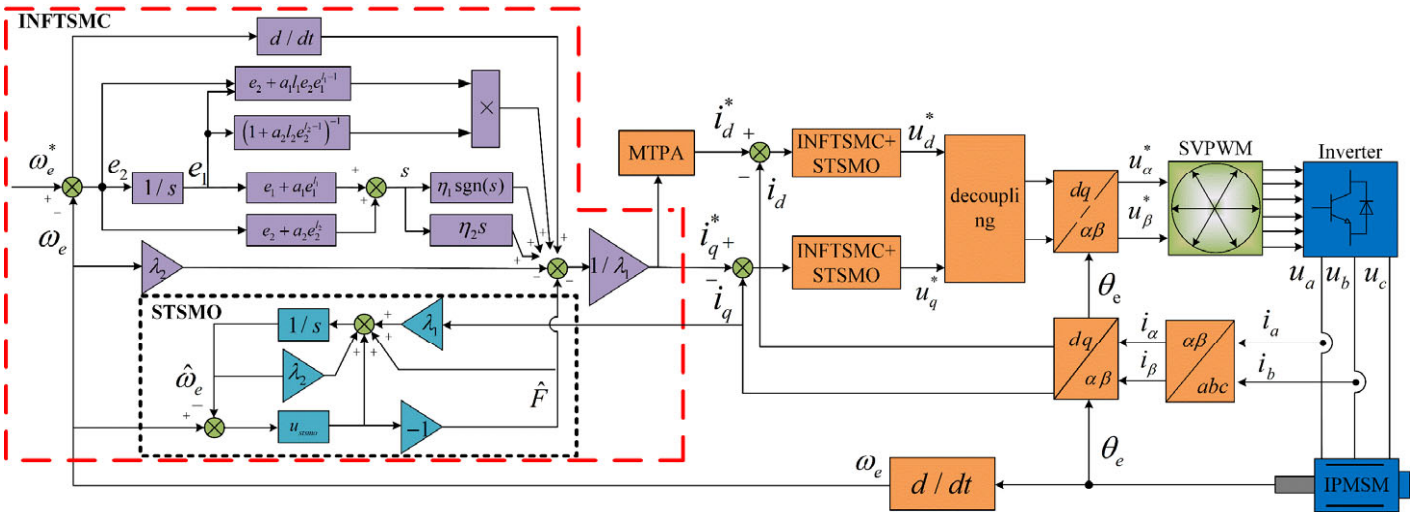

FIGURE 1. The block diagram of INFTSMC + STSMO.

TABLE 1. The parameters of PMSM.

Parameters	Units	Values
Stator resistance/R_s	Ω	2.75
Rated speed/n_N	r/min	1900
Pole number/n_p	pairs	2
q-axis inductance/L_q	H	0.009
d-axis inductance/L_d	H	0.004
Inertia/J	kg·m^2	0.029
Damping coefficient/B	N·m·s/rad	0.001
Magnetic flux/ψ_f	Wb	0.12

TABLE 2. The experimental conditions of PMSM.

Time/s	Change in parameters	Range of change
1.0	R_s/Ω	$2 \rightarrow 2.6$
1.5	ψ_f/Wb	$0.12 \rightarrow 0.09$
2.0	n^*/r/min	$1000 \rightarrow 2000$
2.5	L_d/H	$0.004 \rightarrow 0.0031$
3.0	L_q/H	$0.009 \rightarrow 0.0061$
3.5	B/N · m · s/rad	$0.001 \rightarrow 0.0041$
4.0	J/kg · m^2	$0.029 \rightarrow 0.041$
4.5	T_L/N·m	$15 \rightarrow 20$
5.0	T_L/N·m	$20 \rightarrow 15$

This paper uses saturated function $D(s)$ instead of symbolic function. $D(s)$ is expressed as

$$D(s) = \frac{s}{|s| + \Lambda} \tag{36}$$

where $\Lambda > 0$.

4. ANALYSIS OF EXPERIMENTAL RESULTS

4.1. Analysis of Simulation Results

The proposed INFTSMC + STSMO control algorithm is implemented on a MATLAB/Simulink platform and evaluated through the comparison with conventional PI and SMC + SMO control strategies. Parameters of the PMSM used in the simulation are listed in Table 1, and the experimental conditions are detailed in Table 2. The overall block diagram of the INFTSMC + STSMO scheme is illustrated in Fig. 1.

4.2. Analysis of Simulation Results

Figure 2 presents a simulation-based comparison among the PI, SMC + SMO, and INFTSMC + STSMO control strategies. A comparison of Figs. 2(a) and 2(b) demonstrates that the proposed INFTSMC + STSMO method yields the best performance. Specifically, the PI controller exhibits a significant overshoot in the speed response, while the SMC + SMO approach, despite avoiding overshoot due to its nonlinear control characteristics, requires a longer time to reach the desired speed.

Figures 2(b)–2(d) further illustrate that the output torque and d-q axis currents under INFTSMC + STSMO control remain the most stable, featuring fast response times and minimal oscillations. In contrast, both the PI and SMC + SMO controllers produce transient overshoots and exhibit larger steady-state ripples in torque and current, indicating inferior dynamic and steady-state performance.

Figure 3 presents the observation performance of the sliding mode observer (SMO) and super-twisting sliding mode observer (STSMO). As shown in the figure, the SMO exhibits limited tracking capability for the rotor speed and d-q axis currents of the PMSM drive system, with tracking errors failing to converge stably to zero. In contrast, the STSMO achieves rapid and accurate tracking of the system's reference speed and currents, with its tracking error stably converging to zero. Both SMO and STSMO can effectively estimate the unknown total disturbance term F in the three-loop PMSM control system. However, under composite parameter perturbations, the SMO demonstrates reduced estimation accuracy, while the STSMO maintains precise estimation performance, highlighting its superior robustness to system uncertainties.

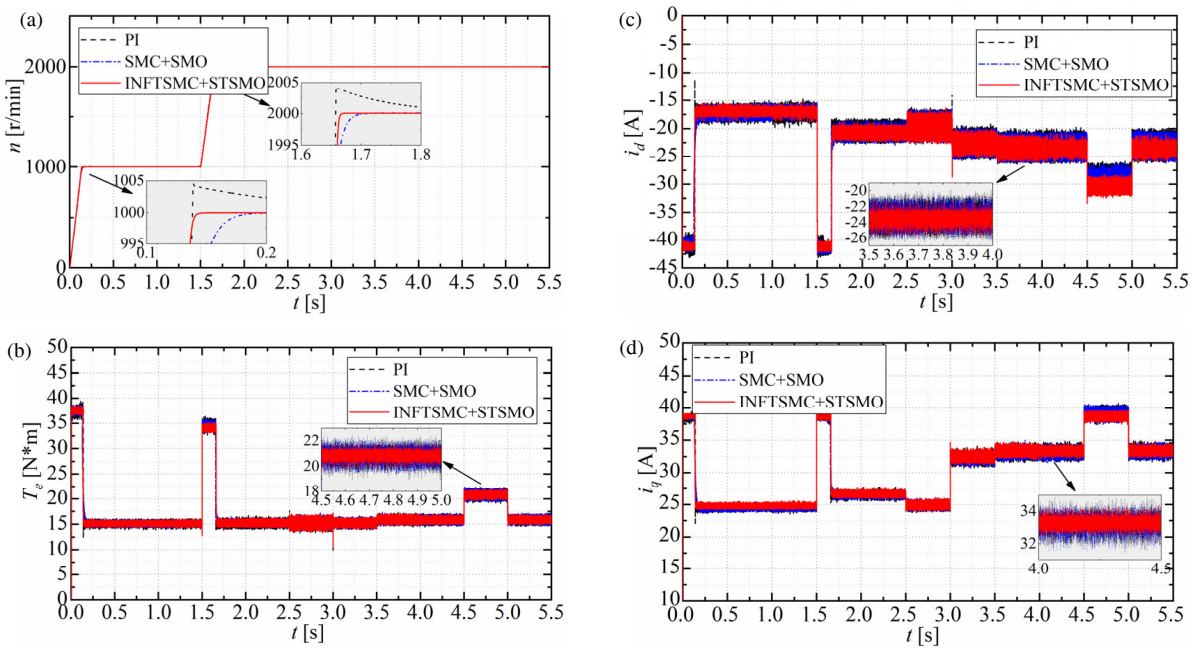

FIGURE 2. The simulation comparison of PI/SMC + SMO/INFTSMC + STSMO. (a) Simulation of n. (b) Simulation of T_e. (c) Simulation of i_d. (d) Simulation of i_q.

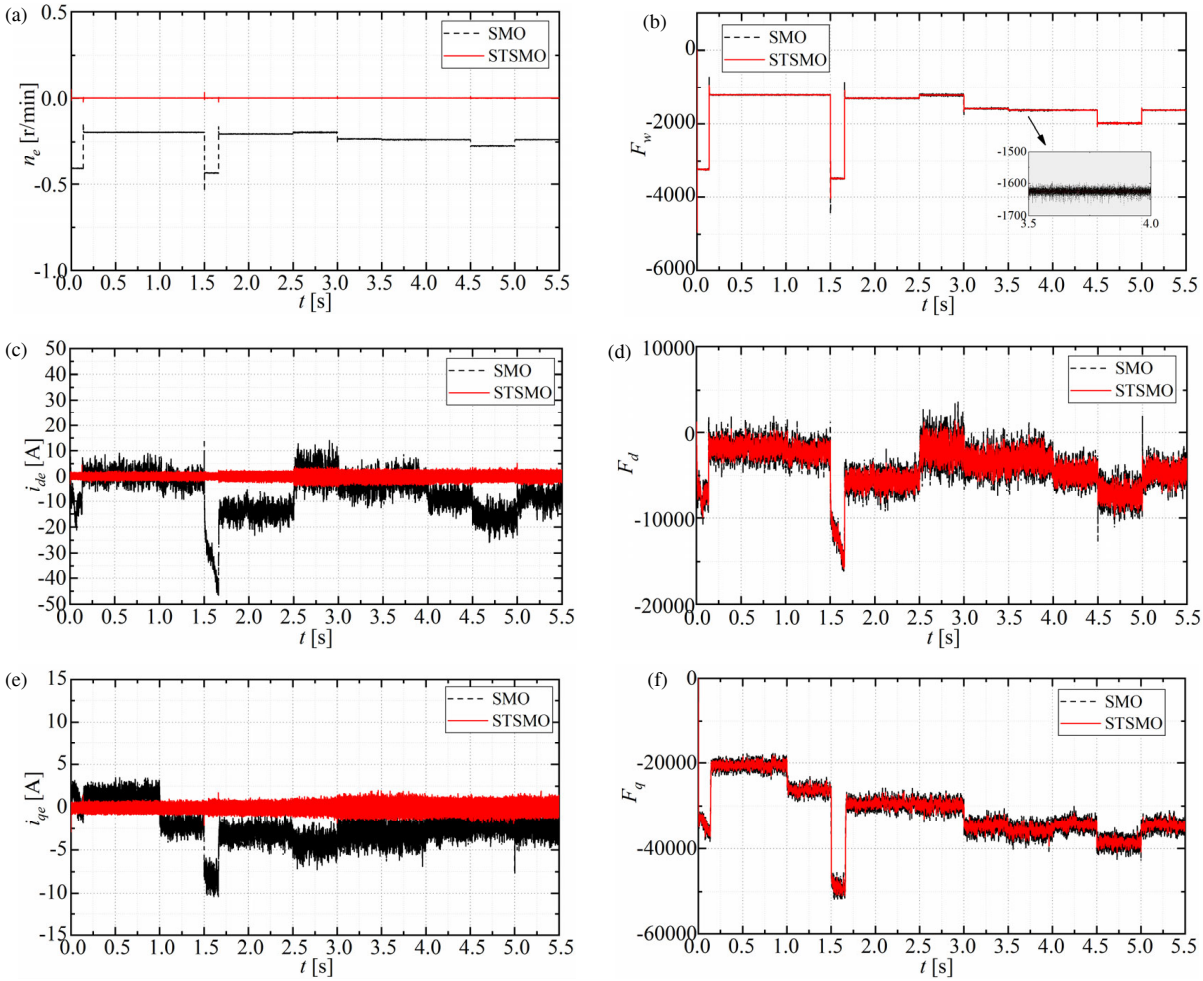

FIGURE 3. The observation results of SMO/STSMO. (a) The error of n. (b) F_w. (c) The error of i_d. (d) F_q. (e) The error of i_q. (f) F_q.

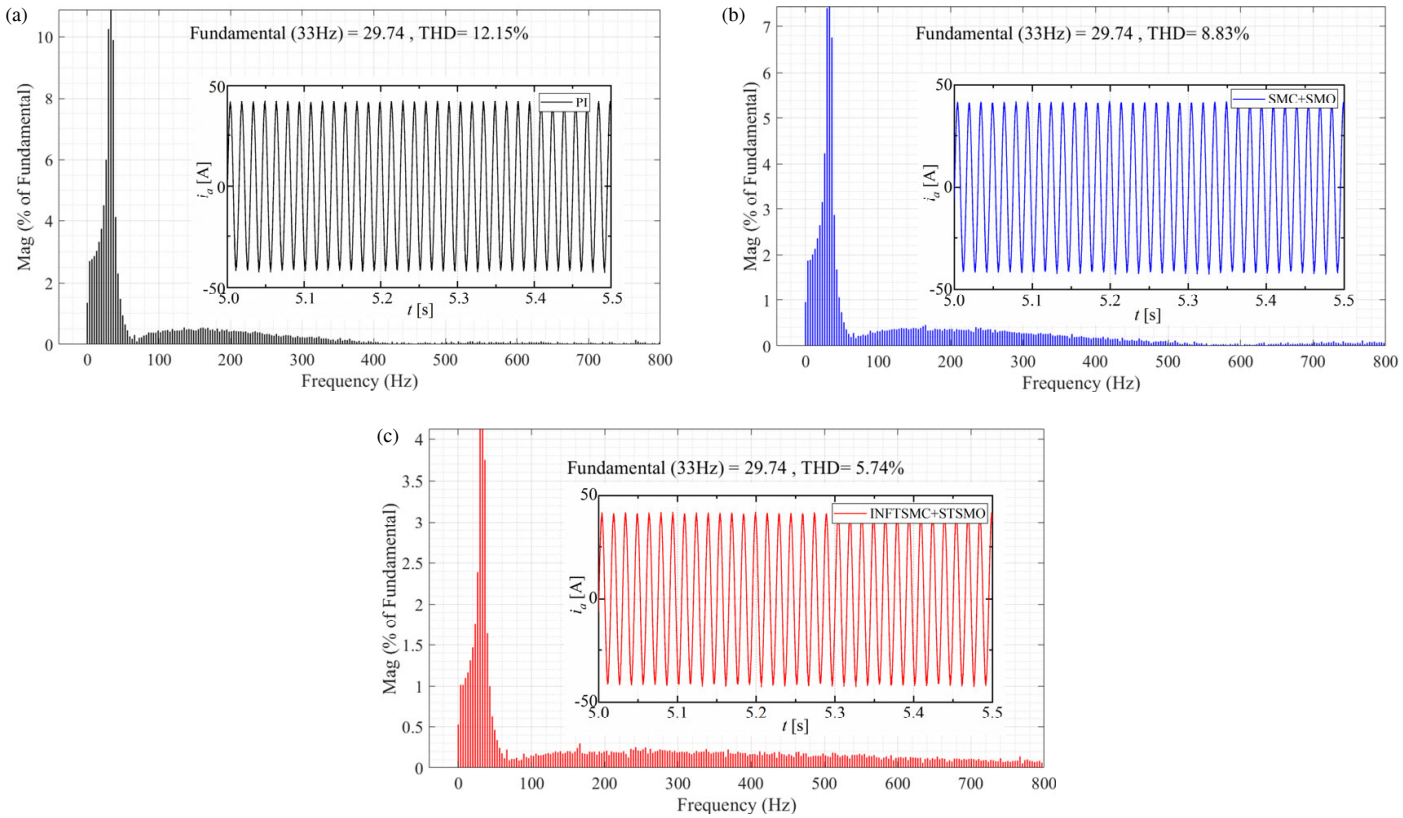

FIGURE 4. The THD analysis of i_a for PI/SMC + SMO /INFTSMC + STSMO. (a) The THD of PI. (b) The THD of SMC + SMO. (c) The THD of INFTSMC + STSMO.

TABLE 3. The comparison of results.

Performance indicators	PI	SMC + SMO	INFTSMC + STSMO
torque pulsation	14.11%	10.01%	6.83%
THD /%	12.15	8.83	5.74
Response time	0.4/0.4	0.18/0.18	0.13/0.15
static differential	0.062	0.0253	0.011

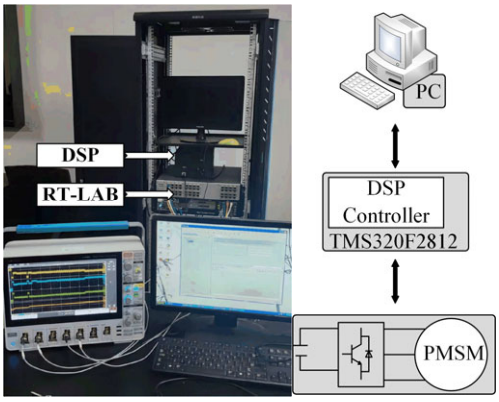

FIGURE 5. The experimental platform of RT-LAB.

Figure 4 illustrates the phase-i_a current waveforms and total harmonic distortion (THD) comparisons for the three control algorithms. As shown in Figs. 4(a)–4(c), the proposed INFTSMC + STSMO method achieves the lowest THD among all strategies and effectively suppresses current pulsations induced by parameter perturbations. This results in improved current quality and enhanced overall performance of the PMSM drive system.

4.3. Analysis of RT-LAB Experimental Results

Figure 5 depicts the RT-LAB real-time hardware-in-the-loop (HIL) experimental platform used in this study. The PMSM drive system was simulated on the RT-LAB platform during the experiments. Fig. 6 presents the experimental waveforms obtained from the PI, SMC + SMO, and INFTSMC + STSMO control algorithms.

Based on the simulation results shown in Figs. 2 and 6, the overall performance of PI and SMC + SMO is limited. Specifically, system convergence speed, output torque stability, d-q axis currents, and total harmonic distortion (THD) values fail to meet the demands of high-performance control. In contrast, the proposed INFTSMC + STSMO method effectively overcomes these shortcomings, enabling the PMSM drive system

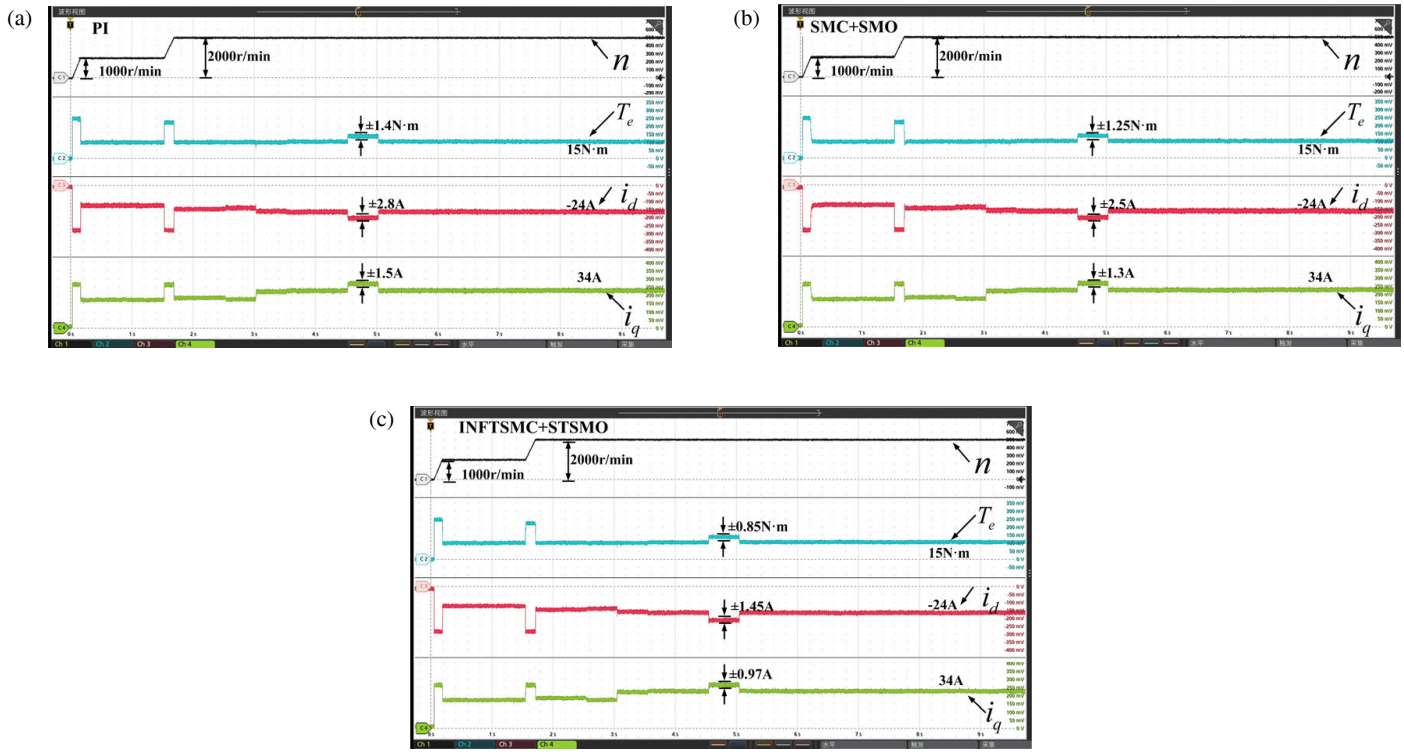

FIGURE 6. The RT-LAB experimental waveforms. (a) PI. (b) SMC + SMO. (c) INFTSMC + STSMO.

to achieve high-precision control. Table 3 summarizes the performance comparison among PI, SMC + SMO, and INFTSMC + STSMO.

5. CONCLUSION

To address the limitations of PI and SMC + SMO in achieving high-quality current control, this paper optimizes the speed-current loops of a PMSM drive system and proposes a continuous INFTSMC + STESMO control method. The proposed composite control approach reduces a number of tuning parameters and mitigates system vibrations. Furthermore, it enhances control performance, improves the robustness of the PMSM drive system, and accelerates the dynamic response

ACKNOWLEDGEMENT

This work was supported by the National Natural Science Foundation of China under Grant 62303178, the Natural Science Foundation of Hunan Province Grant 2023JJ50193, and Postgraduate Scientific Research Innovation Project of Hunan Province Grant CX20231107.

REFERENCES

[1] He, Y., K. Zhao, Z. Yi, and Y. Huang, "Improved terminal sliding mode control of PMSM dual-inertia system with acceleration feedback based on finite-time ESO," *Progress In Electromagnetics Research M*, Vol. 134, 21–30, 2025.

[2] Wen, D., C. Liu, Y. Zhang, and Z. Cheng, "Simplified duty cycle modulation model predictive current control of PMSM without cost function," *Progress In Electromagnetics Research C*, Vol. 156, 147–159, 2025.

[3] Zhang, Y., P. Yang, K. Cao, Y. Gao, G. Tang, and Q. Chen, "Improved model predictive torque control strategy incorporating decoupled sliding mode disturbance observer for PMSM," *Progress In Electromagnetics Research C*, Vol. 153, 105–117, 2025.

[4] Cheng, S., H. Wang, and Y. Jiang, "Improved orthogonal flux corrector-based rotor flux estimation in PMSM sensorless control," *Progress In Electromagnetics Research Letters*, Vol. 121, 57–63, 2024.

[5] Li, X., J. Liu, K. Zhao, Y. Yin, and L. Zou, "An improved model-free sliding mode control algorithm of super-twisting for SPMSM," *Progress In Electromagnetics Research C*, Vol. 135, 195–210, 2023.

[6] Yi, Z., X. Li, Y. Yin, J. Liu, and K. Zhao, "Deep flux weakening control of IPMSM based on d-axis current error integral regulator," *Progress In Electromagnetics Research M*, Vol. 118, 163–175, 2023.

[7] Li, X., J. Liu, Y. Yin, and K. Zhao, "Improved super-twisting non-singular fast terminal sliding mode control of interior permanent magnet synchronous motor considering time-varying disturbance of the system," *IEEE Access*, Vol. 11, 17 485–17 496, 2023.

[8] Zhao, K., W. Liu, T. Yin, R. Zhou, and W. Dai, "Model-free sliding mode control for PMSM drive system based on ultra-local model," *Energy Engineering: Journal of the Association of Energy Engineers*, Vol. 119, No. 2, 767–780, 2022.

[9] Li, X., J. Liu, K. Zhao, Y. Yin, and L. Zou, "Improved non-singular fast terminal sensor-less sliding mode control of IPMSM considering external disturbance and parameter perturbation," *Progress In Electromagnetics Research B*, Vol. 102, 81–98, 2023.

[10] Wang, F., Y. Wei, H. Young, D. Ke, H. Xie, and J. Rodríguez, "Continuous-control-set model-free predictive fundamental current control for PMSM system," *IEEE Transactions on Power Electronics*, Vol. 38, No. 5, 5928–5938, 2023.

[11] Yim, J., S. You, Y. Lee, and W. Kim, "Chattering attenuation disturbance observer for sliding mode control: Application to permanent magnet synchronous motors," *IEEE Transactions on Industrial Electronics*, Vol. 70, No. 5, 5161–5170, 2023.

[12] Xu, W., A. K. Junejo, Y. Liu, and M. R. Islam, "Improved continuous fast terminal sliding mode control with extended state observer for speed regulation of PMSM drive system," *IEEE Transactions on Vehicular Technology*, Vol. 68, No. 11, 10 465–10 476, 2019.

[13] Hou, Q., S. Ding, and X. Yu, "Composite super-twisting sliding mode control design for PMSM speed regulation problem based on a novel disturbance observer," *IEEE Transactions on Energy Conversion*, Vol. 36, No. 4, 2591–2599, 2021.

[14] Wang, Z., J. Chai, X. Xiang, X. Sun, and H. Lu, "A novel online parameter identification algorithm designed for deadbeat current control of the permanent-magnet synchronous motor," *IEEE Transactions on Industry Applications*, Vol. 58, No. 2, 2029–2041, 2021.

[15] Wu, Y.-J., J.-X. Zuo, and L.-H. Sun, "Adaptive terminal sliding mode control for hypersonic flight vehicles with strictly lower convex function based nonlinear disturbance observer," *ISA Transactions*, Vol. 71, 215–226, 2017.

[16] Merzouki, T. and M. Rachek, "High accurate PMSM computation model based on strongly coupled magnetic field and multiturn electric winding circuits using the time-stepping finite element," *Progress In Electromagnetics Research C*, Vol. 153, 13–23, 2025.

[17] Zhou, D. and X. Wang, "Deadbeat control of permanent magnet synchronous motorized spindle based on improved parameter identification algorithm," *Progress In Electromagnetics Research C*, Vol. 153, 81–86, 2025.

[18] Guo, X., S. Huang, K. Lu, Y. Peng, H. Wang, and J. Yang, "A fast sliding mode speed controller for PMSM based on new compound reaching law with improved sliding mode observer," *IEEE Transactions on Transportation Electrification*, Vol. 9, No. 2, 2955–2968, 2023.

[19] Yang, Y., M. Deng, S. Li, and Y. Zhang, "Based on fast non-singular terminal sliding of PMSM model-free control," *Progress In Electromagnetics Research C*, Vol. 137, 139–153, 2023.

[20] Kang, E., H. Yu, and K. Han, "No nlinear gain non-singular fast terminal sliding mode control for permanent magnet synchronous motors," *Electric Machines and Control*, Vol. 28, No. 5, 73–81, 2024.

[21] Zhao, X. and D. Fu, "Adaptive neural network nonsingular fast terminal sliding mode control for permanent magnet linear synchronous motor," *IEEE Access*, Vol. 7, 180 361–180 372, 2019.

[22] Li, X., Y. Yin, Y. Zhou, W. Liu, and K. Zhao, "The non-singular fast terminal sliding mode control of interior permanent magnet synchronous motor based on deep flux weakening switching point tracking," *Energy Engineering*, Vol. 120, No. 2, 277, 2023.

[23] Zhao, K. H., W. K. Dai, R. R. Zhou, A. Leng, W. Liu, P. Qiu, G. Huang, and G. Wu, "Novel model-free sliding mode control of permanent magnet synchronous motor based on extended sliding mode disturbance observer," *Proceedings of the CSEE*, Vol. 42, No. 6, 2375–2386, 2022.

[24] Wang, J., R. Zhou, and J. Liu, "New non-singular fast terminal sliding mode control of permanent magnet synchronous motor based on super-twisting sliding mode observer," *Progress In Electromagnetics Research C*, Vol. 146, 151–162, 2024.